Research Square

Preprints are preliminary reports that have not undergone peer review.
They should not be considered conclusive, used to inform clinical practice,
or referenced by the media as validated information.

Hydroclimate associations do not ensure temporal or spatial transferability of positive Anopheles catch intensity in southwestern Colombia

Johan Ceballos
Universidad Nacional de Colombia
Andrea Camila Silva Cordero
ansilvaco@unal.edu.co

Universidad Nacional de Colombia

Research Article

Keywords: Anopheles albimanus, Anopheles neivai, biometeorology, hydroclimate, spatial transferability, zero-truncated negative binomial model

Posted Date: October 21st, 2026

DOI: https://doi.org/10.21203/rs.3.rs-10933765/v1

License: This work is licensed under a Creative Commons Attribution 4.0 International License. Read Full License

Additional Declarations: No competing interests reported.

Abstract

Biometeorological associations are often treated as potential surveillance signals, but statistical detection does not establish transfer across years or sites. We reanalysed 1,502 openly published positive-catch records representing 229,394 *Anopheles* mosquitoes collected in 25 rural localities in southwestern Colombia from January 2021 to March 2023 and linked them to daily NASA POWER temperature, humidity, and precipitation. Species-specific zero-truncated negative binomial models included sampling effort as an offset, cluster-robust uncertainty, frozen temporal evaluation (train 2021, validate 2022, test January–March 2023), and leave-one-sampling-unit-out transfer. *Anopheles albimanus* and *Anopheles neivai* passed prespecified gates. After Benjamini–Hochberg correction across eight species-by-climate coefficients, *An. neivai* positive-catch intensity remained positively associated with event temperature (standardized beta = 0.453; q = 0.047) and 14-day antecedent rainfall (beta = 0.132; q = 0.044). The negative *An. albimanus* temperature coefficient was nominally supported but not false-discovery-rate robust (beta = − 1.482; q = 0.079). Predictive transfer was mixed: spatial rank correlations were 0.342 and 0.358, and the 2023 *An. albimanus* model overpredicted the aggregate catch by approximately 6.2-fold. Thus, detectable hydroclimate associations did not ensure temporal or spatial transferability. Positive-only sampling, three coarse climate cells, unobserved intervention phase, and a three-month test period constrain causal and operational interpretation. Multiplicity-aware inference and blocked validation should precede operational use of climate-informed vector models.

Introduction

Mosquito abundance, host-seeking activity, development, and survival respond to atmospheric conditions through nonlinear and species-specific mechanisms. Temperature can accelerate development and pathogen processes within a viable range, whereas rainfall can create or flush larval habitats and its effects depend on landscape, timing, and vector ecology (Mordecai et al. 2019). These dependencies make biometeorological information relevant to vector surveillance, but they also make simple extrapolation hazardous: an association estimated within a particular species, site, or season may not persist elsewhere.

The Colombian Pacific lowlands combine high rainfall, humidity, ecological heterogeneity, and multiple locally important malaria vectors. *Anopheles albimanus* is a major coastal vector with broad ecological tolerance, while *Anopheles neivai* is closely associated with forest bromeliads and mangrove environments and has documented anthropophilic biting in the Pacific region (Solarte et al. 1996; Montoya-Lerma et al. 2011; Escovar et al. 2013). Earlier work reported a direct relationship between accumulated monthly rainfall and *An. neivai* larval fluctuation (Murillo et al. 1988), and entomological–climatic analyses in Colombia have shown that temperature and rainfall can carry useful but context-dependent information (Ruiz et al. 2006). Distribution studies likewise show that *Anopheles* species occupy heterogeneous settings within the Pacific region (Ahumada et al. 2016; Fuller et al. 2012).

Public biodiversity archives now allow independent reanalysis of structured entomological records. Darwin Core improves interoperability by standardizing occurrence and event fields (Wieczorek et al. 2012), but occurrence archives may contain only positive species records. Treating such data as if zeros had been observed would change the estimand and violate the sampling support. A zero-truncated count likelihood instead conditions on a positive catch and estimates variation in positive-catch intensity (Zeileis et al. 2008). This distinction is fundamental: the resulting model cannot estimate occurrence probability, total population abundance, intervention efficacy, malaria transmission, or causal climate effects.

We used an openly published Darwin Core dataset from protected human-attractant collections in 25 localities of Guapi, Timbiquí, and Santa Bárbara (Ahumada et al. 2021). We tested three prespecified hypotheses. First, recent rainfall would be positively associated with *An. neivai* positive-catch intensity, consistent with its bromeliad-linked larval ecology. Second, temperature associations would differ between *An. neivai* and *An. albimanus* rather than follow a single cross-species direction. Third, adding hydroclimate variables to seasonal and administrative controls would improve at least the ranking of positive-catch intensity outside the training year, although calibration could remain site-dependent. Beyond coefficient estimation, we explicitly audited temporal and spatial transfer. This distinction is central because successful internal fit and random cross-validation do not establish geographic or temporal transferability (Wenger and Olden 2012; Roberts et al. 2017; Meyer et al. 2018).

Materials and methods

Study design and source data

This was a secondary, observational analysis of version 1.0 of the occurrence dataset “Especies del género *Anopheles* (Diptera: Culicidae) asociadas al domicilio humano en 25 localidades de los municipios de Timbiquí, Guapi y Santa Bárbara…”, published by the

Instituto Nacional de Salud (Ahumada et al. 2021; https://doi.org/10.15472/kftrcn). The pinned Darwin Core archive had SHA-256 7ab6376eb3a8279b4f634507c97d7a820027688cbb9e7b24f4c6e97a0f02ed34. It contains 1,502 positive occurrence records totaling 229,394 mosquitoes collected from January 2021 through March 2023 in 25 rural localities. Source metadata describe trained collectors using protected human attractant catches inside and outside dwellings. Each analytical row represented a positive species count aggregated within a published event; absence events were unavailable and were not reconstructed.

The initial target taxa were *An. albimanus*, *An. neivai*, and *An. apicimacula*. The response was individualCount. Sampling exposure was parsed from the published samplingEffort field as hours per night multiplied by number of nights. The primary quality-control rules required a positive integer count, a valid event date or date interval, interpretable effort, target-species membership, and coordinates. Dates were never imputed. When row-level coordinates were missing, coordinates were filled only if the same parentEventID had a single unambiguous published coordinate pair. Two later rows with analytically identical fields but different identifiers were retained in the primary analysis and removed in a sensitivity analysis.

Meteorological exposure

Daily meteorological fields were downloaded automatically through the National Aeronautics and Space Administration Prediction Of Worldwide Energy Resources (NASA POWER) point application programming interface (NASA POWER Project 2026). Coordinates were assigned to the nearest 0.5° grid cell, yielding three cells in the study domain. Across eligible records there were 56 parentEventID–grid assignments: 23 at 2.5° N, 78.0° W; 18 at 2.5° N, 77.5° W; and 15 at 3.0° N, 77.5° W. One parent event crossed two grid cells. We used mean 2-m air temperature (T2M, °C), mean 2-m relative humidity (RH2M, %), and corrected precipitation (PRECTOTCORR, mm day − 1). For each record, temperature, humidity, and precipitation were averaged across the published sampling interval. Antecedent rainfall was the accumulated precipitation during the 14 complete days before sampling began. The 14-day window was chosen a priori as a simple, biologically interpretable recent-rainfall exposure and was not selected by searching alternative lags. Event-period variables describe contemporaneous adult collection conditions; they are not assumed to represent the complete larval or generational exposure history. Climate completeness had to be at least 95% for both the event interval and antecedent window; observed completeness was 100%. Event day of year was represented by sine and cosine harmonics.

Prespecified data gates

Species proceeded to modelling only if they had at least 150 eligible records overall, 100 training records, 100 validation records, 40 test records, 20 sampling-unit clusters overall, and eight clusters within each temporal split. The maximum absolute correlation among climate predictors could not exceed 0.95, and the design matrix had to be full rank with condition number below 10^6. Model convergence was also required. These gates were fixed before the final run and prevented post-result relaxation of sample requirements.

Zero-truncated negative binomial model

For each eligible species, positive counts were modelled with a zero-truncated negative binomial type 2 (ZTNB2) likelihood. Let fNB2(y; μ, θ) denote the negative binomial mass with mean μ and variance μ + μ²/θ. Conditioning on an observed positive catch gives:

$$Pr(Y = y \mid Y > 0) = fNB2(y;\, \mu\,,\, \theta\,) \,/\, [1 - fNB2(0;\, \mu\,,\, \theta\,)], \quad y = 1,\, 2,\, \ldots$$

The log mean was log(μi) = log(totalEffortHoursi) + xi⊠β, where the offset represents published exposure and xi includes standardized event temperature, event relative humidity, event mean precipitation, 14-day antecedent rainfall, sine and cosine season terms, and fixed indicators for Santa Bárbara and Timbiquí, with Guapi as reference. Because the likelihood is conditional on positivity, exp(beta) describes a multiplicative change in the underlying negative-binomial mean parameter, not a direct occurrence probability or an unconditional abundance ratio.

Maximum likelihood estimation used three dispersion starting values (0.25, 1, and 5) and retained the finite solution with the lowest negative log likelihood. Cluster-robust sandwich covariance matrices were calculated by parentEventID to allow within-unit dependence (Cameron and Miller 2015). Four climate variables were standardized with 2021 training means and standard deviations during temporal validation. Final coefficient models used all eligible years and all-year standardization. A baseline model retained the offset, intercept, season terms, and administrative indicators but omitted hydroclimate terms.

Temporal validation, spatial transfer, and sensitivity analyses

The temporal split was frozen by year: 2021 for training, 2022 for validation, and January–March 2023 for testing. Performance measures were mean absolute error of positive-catch rate, root mean squared error of log(1 + positive-catch rate), Spearman rank correlation, the ratio of observed to predicted total count, and mean conditional log likelihood. Full and baseline models were compared on the same records. Final all-year full and baseline models were additionally compared by Akaike information criterion.

Spatial transfer was evaluated by leaving out one parentEventID at a time, refitting the full model, and predicting the omitted unit. Folds with fewer than two held-out rows or fewer than 150 training rows were not attempted. This blocked strategy was used because random row-level cross-validation can overstate performance when data are spatially or hierarchically dependent (Roberts et al. 2017), and because evaluation should match the intended prediction task (Meyer et al. 2018). Cluster bootstrap uncertainty for coefficient stability used 200 parentEventID resamples. Primary coefficient inference relied on the cluster-robust sandwich intervals and multiplicity adjustment; the 200-replicate bootstrap was an exploratory direction-and-stability check rather than a high-precision tail-probability procedure. Percentile intervals were reported when at least 80% of replicates converged. Sensitivity analyses excluded exact analytical duplicate extras, excluded coordinate-imputed rows, or restricted events to intervals of 14 days or less. After the primary pipeline was locked, uncertainty for spatial metrics was summarized by 2,000 deterministic resamples of held-out units, conditional on the existing fold predictions and without refitting; these intervals therefore represent variation among held-out units, not training-model uncertainty.

Multiplicity, effect scale, collinearity, and model diagnostics

Because eight species-by-climate coefficients were examined, we added a secondary Benjamini–Hochberg false-discovery-rate adjustment across the complete family of eight two-sided cluster-robust tests (Benjamini and Hochberg 1995). Raw p values and adjusted q values are reported together; this post hoc safeguard does not convert the analysis into a confirmatory trial. Standardized climate coefficients were also translated to prespecified, interpretable increments using each species' all-year predictor standard deviation. For temperature, the multiplier was reported per 1°C together with the observed range. Collinearity was summarized by the maximum pairwise climate correlation and by variance inflation factors in which each climate predictor was regressed on all remaining climate, seasonal, and municipality design columns. The full-design condition number was also reported.

Goodness of fit was evaluated from the zero-truncated negative binomial conditional mean and variance. We examined Pearson residual dispersion, deterministic mid-quantile residuals against normal quantiles, and Pearson residuals against fitted conditional counts (Online Resource 1, Table S9; Online Resource 3, Fig. S1). These diagnostics assess the final all-year fit; they do not replace the frozen temporal and spatial transfer evaluations. Reporting was reviewed against the STROBE checklist, supplied as a related file for editorial assessment.

Software, reproducibility, and use of generative tools

All downloads, quality checks, modelling, analytical tables, status files, and SHA-256 checksums were produced automatically in MATLAB 26.1.0.3346908 (R2026a) Update 5 using seed 20260830. The successful final run started on 31 August 2026 at 14:44:07 and completed all 10 stages at 14:52:05. Additional diagnostics were derived deterministically from the locked analytical panel, coefficient table, and spatial fold predictions without downloading data or refitting the primary models; a toolbox-free MATLAB post-processing script is supplied. Journal artwork was rendered from verified comma-separated outputs using Python 3.12.13, pandas 2.2.3, Matplotlib 3.10.8, and Pillow 12.3.0. During manuscript preparation, ChatGPT (OpenAI) assisted with English-language editing, document organization, and preparation and review of reproducibility and post-processing code. It was not used to generate the source data or primary model outputs. The authors verified the code, calculations, references, figures, and final text and remain responsible for the work.

Results

Data audit and modelling eligibility

The archive audit reproduced all 1,502 source rows and the published total of 229,394 mosquitoes. Twenty rows with missing or invalid dates were excluded, 92 coordinates were recovered from an unambiguous coordinate within the same parent event, and no coordinate remained unresolved. The final analytical panel contained 1,482 positive-catch records. *An. albimanus* contributed 496 records and 52 sampling-unit clusters; *An. neivai* contributed 812 records and 54 clusters. Both passed all gates. *An. apicimacula*

contributed 174 records but failed the required training, validation, and test sizes (Table 1) and was retained only in descriptive summaries.

Table 1
Source audit, temporal sample sizes, and prespecified modelling gates

Species	Source records	Source individuals	Eligible records	2021 train	2022 validation	2023 test	Clusters	Gate
Anopheles albimanus	504	34,424	496	203	229	64	52	Pass
Anopheles neivai	823	194,356	812	329	384	99	54	Pass
Anopheles apicimacula	175	614	174	74	88	12	35	Fail

The 2023 test period covered January–March only. *Anopheles apicimacula* failed ntraining, nvalidation, and ntest thresholds; its exclusion was determined before fitting.

Descriptive positive-catch intensity

Across eligible records, the median positive-catch rate was 0.333 mosquitoes per published sampling hour for *An. albimanus* (interquartile range 0.056–1.583) and 3.486 for *An. neivai* (1.106–8.328). Median sampling exposure was 48 h for both species. Monthly medians varied markedly across the 27-month observation window (Fig. 2), with *An. neivai* generally showing higher positive-catch rates. These trajectories are descriptive because the archive does not include sampling events with zero individuals of a species and sampling was not continuous in every month.

Hydroclimate coefficients

All final full and baseline models converged. Relative to the seasonal–administrative baseline fitted on the same all-year data, the full model reduced Akaike information criterion by 20.48 units for *An. albimanus* (4,404.23 versus 4,424.71) and by 43.62 units for *An. neivai* (10,135.39 versus 10,179.01). These are in-sample fit comparisons and are not evidence of transfer by themselves.

The two species had temperature coefficients with opposite signs, but multiplicity adjustment distinguished their evidential strength. For *An. albimanus*, standardized event temperature was negative (beta = − 1.482, cluster-robust 95% confidence interval − 2.817 to − 0.146; raw p = 0.030), but its Benjamini–Hochberg q value was 0.079. For *An. neivai*, event temperature was positive (beta = 0.453, 0.101 to 0.805; raw p = 0.012; q = 0.047), and 14-day antecedent rainfall was also positive (beta = 0.132, 0.039 to 0.226; raw p = 0.005; q = 0.044). Thus, only the two *An. neivai* coefficients remained below an FDR threshold of 0.05 across the eight tests (Table 2; Fig. 3). The bootstrap intervals for these three nominal signals had the same directions. Bootstrap convergence was 196/200 for *An. albimanus* and 193/200 for *An. neivai*.

Observed event temperature ranged from 22.053 to 27.690°C. On the original scale, a 1°C increase corresponded to a multiplier of 0.412 (95% confidence interval 0.186 to 0.916) in the latent mean parameter for *An. albimanus* and 1.385 (1.075 to 1.784) for *An. neivai*. These are conditional model associations within the observed tropical support, not causal or physiological rate ratios (Online Resource 1, Table S7).

Table 2
Standardized hydroclimate coefficients from final all-year zero-truncated negative binomial models

Species	Predictor	beta	Cluster-robust SE	95% CI	Raw p	BH q (8 tests)	Cluster-bootstrap 95% interval
Anopheles albimanus	Event temperature	-1.482	0.681	-2.817 to -0.146	0.030	0.079	-2.487 to -0.462
Anopheles albimanus	Event relative humidity	-0.511	0.346	-1.188 to 0.167	0.139	0.227	-0.969 to 0.153
Anopheles albimanus	Event mean rainfall	-0.113	0.077	-0.263 to 0.038	0.142	0.227	-0.249 to 0.154
Anopheles albimanus	14-day antecedent rainfall	-0.050	0.145	-0.333 to 0.234	0.731	0.731	-0.377 to 0.299
Anopheles neivai	Event temperature	0.453	0.180	0.101 to 0.805	0.012	0.047	0.056 to 0.856
Anopheles neivai	Event relative humidity	0.100	0.075	-0.048 to 0.247	0.185	0.246	-0.022 to 0.289
Anopheles neivai	Event mean rainfall	0.013	0.035	-0.055 to 0.081	0.703	0.731	-0.051 to 0.215
Anopheles neivai	14-day antecedent rainfall	0.132	0.048	0.039 to 0.226	0.005	0.044	0.060 to 0.284

Climate predictors were standardized within species. Raw p values are two-sided normal approximations from cluster-robust z statistics. BH q values apply the Benjamini–Hochberg procedure jointly to the eight species-by-climate tests. Bootstrap intervals used 200 parentEventID resamples.

Collinearity and all-year fit diagnostics

The prespecified training-set maximum absolute climate correlation was 0.658 for *An. albimanus* and 0.635 for *An. neivai*, well below 0.95. In the all-year matrices, the corresponding maxima were 0.642 and 0.612, both between temperature and relative humidity. When municipality indicators and seasonal harmonics were included, the largest full-design climate variance inflation factor was 3.124 for *An. albimanus* and 2.840 for *An. neivai*; full-design condition numbers were 6.490 and 6.838, respectively (Online Resource 1, Table S8). These values do not indicate severe linear dependence, although they do not remove the risk that coarse-grid temperature marks local or seasonal structure.

Pearson dispersion was 1.378 for *An. albimanus* and 0.976 for *An. neivai*. Mid-quantile residuals had means near zero and standard deviations of 0.968 and 1.018, respectively. The diagnostic plots showed closer overall agreement for *An. neivai* and tail departures for *An. albimanus*, consistent with remaining heterogeneity not captured by the all-year model (Online Resource 1, Table S9; Online Resource 3, Fig. S1).

Temporal validation

Temporal transfer was mixed rather than uniformly improved by hydroclimate covariates. For *An. albimanus*, the full model increased rank correlation over baseline in validation (0.521 versus 0.280) and test (0.331 versus 0.144), but error, aggregate calibration, and mean log score were worse. In the test period, the full model had root mean squared log-rate error 1.257 and an observed/predicted ratio of 0.161, indicating substantial overprediction, compared with 0.931 and 0.337 for baseline.

For *An. neivai*, the full model reduced root mean squared log-rate error in validation (0.900 versus 0.961) and test (0.789 versus 0.826). It improved validation rank correlation (0.317 versus 0.160) but not test rank correlation (0.277 versus 0.294). Test aggregate calibration was close to one for both models and slightly closer for the full model (0.982 versus 0.926); mean log scores were nearly equal and marginally favored baseline (Table 3; Fig. 4). These fixed-split metrics are descriptive point estimates rather than formal pairwise significance tests. Thus, coefficient-level support did not translate into consistent superiority across predictive criteria.

Table 3
Frozen temporal validation of full hydroclimate and seasonal–administrative baseline models

Species	Split	Model	n	MAE rate	RMSE log-rate	Spearman	Observed/predicted	Mean log score
Anopheles albimanus	Validation	Full	229	3.119	0.983	0.521	0.562	-4.450
Anopheles albimanus	Validation	Baseline	229	2.271	0.873	0.280	0.884	-4.443
Anopheles albimanus	Test	Full	64	4.111	1.257	0.331	0.161	-4.139
Anopheles albimanus	Test	Baseline	64	1.851	0.931	0.144	0.337	-4.066
Anopheles neivai	Validation	Full	384	4.853	0.900	0.317	1.668	-6.583
Anopheles neivai	Validation	Baseline	384	5.016	0.961	0.160	1.385	-6.504
Anopheles neivai	Test	Full	99	3.231	0.789	0.277	0.982	-6.323
Anopheles neivai	Test	Baseline	99	3.217	0.826	0.294	0.926	-6.316

Validation = 2022; test = January–March 2023. Lower MAE and RMSE are better; Spearman closer to 1 is better; observed/predicted closer to 1 is better; less-negative mean log score is better.

Leave-one-sampling-unit-out transfer and sensitivity

All attempted spatial folds converged. The leave-one-unit-out procedure generated predictions for 483/496 *An. albimanus* records (97.4%) across 39 attempted units and 801/812 *An. neivai* records (98.6%) across 43 attempted units. Unattempted units had fewer than two held-out rows. Spatial rank correlations were modest: 0.342 for *An. albimanus* and 0.358 for *An. neivai*. Conditional 95% held-out-unit resampling intervals were 0.056 to 0.578 and 0.201 to 0.506, respectively. The observed/predicted ratio was 0.692 for *An. albimanus*, indicating aggregate overprediction, and 1.013 for *An. neivai* (Table 4; Fig. 5; Online Resource 1, Table S10). The intervals quantify variation among held-out units under locked fold predictions and do not include refitting uncertainty.

Table 4
Leave-one-parentEventID-out spatial transfer of full hydroclimate models

Species	Predictions	Eligible-record prediction coverage	Converged/attempted folds	MAE rate	RMSE log-rate	Spearman (unit-resampling 95% CI)	Observed/predicted	Mean log score
Anopheles albimanus	483	97.4%	39/39	2.738	0.927	0.342 (0.056–0.578)	0.692	-4.596
Anopheles neivai	801	98.6%	43/43	4.292	0.901	0.358 (0.201–0.506)	1.013	-6.273

Eligible-record prediction coverage is the fraction of eligible species records receiving an out-of-unit prediction. Folds with fewer than two held-out records were not attempted. The separate source output variable named coverage was a fold-convergence fraction and was not interpreted as interval coverage.

Sensitivity analyses preserved the positive temperature coefficient for *An. neivai* in every scenario. Its antecedent-rainfall coefficient remained positive with confidence intervals excluding zero after removing duplicate extras and coordinate-imputed rows, but the interval crossed zero when event duration was restricted to 14 days or less (beta = 0.163, 95% confidence interval − 0.037 to 0.363). For *An. albimanus*, the negative temperature coefficient was stable after removing coordinate-imputed rows (beta = − 1.687, − 2.471 to − 0.903) but its interval also crossed zero in the short-event subset (beta = − 0.948, − 1.918 to 0.022). These attenuations indicate that interval construction is an important source of uncertainty.

Discussion

The main contribution of this study is the empirical separation of detectable biometeorological association from predictive transfer. Hydroclimate coefficients improved in-sample fit, yet the full models did not consistently outperform a seasonal–administrative baseline in a later year and retained only modest rank correlations when transferred to held-out sampling units. This result cautions against treating a statistically detectable mosquito–climate coefficient as an operational surveillance signal without structured out-of-sample evaluation.

Multiplicity-aware inference also changed the strength, though not the direction, of the coefficient-level interpretation. Event temperature and 14-day antecedent rainfall for *An. neivai* remained below an FDR threshold of 0.05, whereas the negative temperature coefficient for *An. albimanus* was supported by its unadjusted interval but not after correction across the eight species-by-climate tests. The signs of the two temperature coefficients were opposed within the observed data, but only the *An. neivai* temperature association was FDR-robust. The positive antecedent-rainfall result for *An. neivai* was consistent with the a priori hypothesis and with earlier observations linking rainfall to larval abundance in bromeliad habitats (Murillo et al. 1988).

The temperature coefficients should not be read as universal physiological responses. Event temperature ranged from 22.053 to 27.690°C, and the estimated original-scale multipliers per 1°C were 0.412 for *An. albimanus* and 1.385 for *An. neivai*. Although maximum all-year climate correlations were only 0.642 and 0.612 and all climate variance inflation factors were below 2.30, temperature may still mark species-specific seasonal or local conditions that were not represented explicitly. The two species differ in larval habitats, biting ecology, and spatial distribution (Montoya-Lerma et al. 2011; Escovar et al. 2013; Naranjo-Díaz et al. 2014). Mechanistic thermal relationships are commonly nonlinear and vary across mosquito–pathogen systems (Mordecai et al. 2019); a linear coefficient over this narrow humid-tropical support cannot define a thermal optimum or justify extrapolation beyond the observed range.

The antecedent-rainfall result for *An. neivai* is biologically plausible. Rainwater retained by bromeliads can influence larval habitat volume, and a direct rainfall–larval relationship has been reported on the Colombian Pacific coast (Murillo et al. 1988). However, the primary analysis averages climate over date intervals that often spanned multiple days. When the analysis was restricted to intervals of 14 days or less, the rainfall estimate remained positive but its uncertainty crossed zero. The temperature estimate for *An. albimanus* weakened in the same way. These sensitivity results support describing both patterns as associations that depend partly on the precision of event timing, rather than as definitive climate effects.

The transfer audit adds information that coefficient tables alone cannot provide. In-sample Akaike information criterion favored the full models, but temporal calibration and log scores did not consistently improve. Spatial predictions retained only modest ordering of positive-catch rates, even though almost all records received an out-of-unit prediction. This divergence is compatible with site-specific unmeasured drivers, coarse meteorological support, nonstationary sampling conditions, and differences among parent events. The three POWER cells provided some spatial contrast but cannot resolve microclimate among 25 localities; spatial holdout therefore tests transfer of the complete fitted relationship among sampling units, not transfer across independent fine-resolution climate surfaces. More generally, statistical validation is only informative when its resampling structure resembles the intended application (Wenger and Olden 2012; Roberts et al. 2017; Meyer et al. 2018).

The severe 2023 overprediction for *An. albimanus* deserves particular attention. The full model predicted approximately 6.2 times the observed aggregate count, but broad temperature extrapolation was not the dominant explanation: the 2023 test mean was close to the training mean and only 7.8% of test temperatures fell below the training minimum. Both the full and baseline models overpredicted, while the mean observed positive-catch rate declined from 2.127 in training to 0.747 in testing. Median published effort was also greater in testing (48 h versus 36 h); because effort entered as a proportional offset, greater recorded exposure increased predicted counts even when the catch process had shifted. The negative temperature coefficient could further amplify predictions for cooler test observations. These patterns point to temporal nonstationarity and unobserved operational or intervention changes as plausible contributors, rather than establishing any single mechanism.

All-year residual diagnostics were broadly reassuring for *An. neivai* and indicated remaining heterogeneity for *An. albimanus*. Pearson dispersion was close to one for *An. neivai* but moderately above one for *An. albimanus*, whose mid-quantile plot also showed tail departures. These checks do not invalidate the fitted conditional model, but they reinforce the restrained interpretation of the *An. albimanus* coefficient and the greater importance of blocked predictive evaluation.

Limitations

First, every source occurrence had status “present,” so the analysis conditions on detecting a species. It cannot estimate the probability of a zero catch, geographic occurrence, or unconditional abundance. Positive-catch rates may differ from population density because sampling conditions and human-attractant activity affect capture. Second, the source records arose from a project evaluating long-lasting insecticidal nets and indoor residual spraying, but the Darwin Core core did not provide an unambiguous intervention arm or phase. Intervention and other operational changes may therefore confound year, site, and climate associations. The present analysis must not be used to estimate intervention effects.

Third, NASA POWER linked the study area to only three 0.5° grid cells, with 23, 18, and 15 parentEventID–grid assignments. The data provide daily temporal variation and limited cell-level spatial contrast but cannot represent household-scale rainfall, humidity, or larval-habitat conditions. Fourth, the test set covers only January–March 2023 and one seasonal segment; it is not a full-year prospective test, so the temporal-transfer findings should not be generalized to all seasons. Fifth, the short-event sensitivity reduced sample size and precision. Sixth, the Benjamini–Hochberg adjustment was added after the primary pipeline was locked and should therefore be interpreted as a transparent multiplicity safeguard rather than a prespecified confirmatory analysis. Seventh, the 200-replicate coefficient bootstrap was exploratory, and the spatial metric intervals are conditional on locked fold predictions. Finally, cluster-robust inference, blocked evaluation, and residual diagnostics reduce particular forms of overconfidence but cannot recover omitted covariates or establish causality.

Implications for biometeorological surveillance

The results support species-specific treatment of hydroclimate in vector surveillance. A pooled “mosquito” response would obscure the differing temperature signs and the FDR-robust rainfall signal for *An. neivai*. At the same time, these data do not support operational deployment. At minimum, a candidate climate-informed surveillance model should be evaluated on complete sampling events including zeros, compared with a deployment-relevant non-climatic baseline, tested in temporally forward and spatially external data, assessed for ranking and calibration, and accompanied by uncertainty and explicit failure criteria. Future work should retain intervention arm and phase, household or trap identifiers, standardized collection conditions, micro-loggers or higher-resolution validated meteorological products, and full annual cycles. Because future climates may move beyond the narrow 22.053–27.690°C support observed here, climate-change projections would require mechanistic or nonlinear models and external validation rather than extrapolation of these linear coefficients. Regional risk models and climate-informed vector studies provide useful context, but their predictions remain task- and scale-dependent (Adde et al. 2016; Piedrahita et al. 2020).

Conclusions

Positive *Anopheles* catch intensity in southwestern Colombia showed species-specific hydroclimate patterns, but the strength of those patterns depended on the inferential and validation lens. Temperature and antecedent rainfall for *An. neivai* remained supported after correction across eight climate tests; the negative *An. albimanus* temperature coefficient was nominal but not FDR-robust. Hydroclimate terms improved in-sample fit without producing consistently better predictions across years or sampling units, and *An. albimanus* calibration deteriorated sharply in the short 2023 test. The practical message is therefore not that climate is uninformative, but that an association becomes operationally credible only after it survives multiplicity control, a deployment-relevant baseline, forward temporal testing, spatial transfer, calibration checks, and uncertainty assessment. Positive-only data can support transparent conditional reanalysis, but not claims about absence, unconditional abundance, intervention efficacy, malaria risk, or future-climate response.

Statements and Declarations

Acknowledgements

The authors acknowledge the Instituto Nacional de Salud, the VectorLink Colombia project, the field teams, data managers, and all contributors who generated and published the source entomological dataset. The source dataset is reused under its Creative Commons Attribution–NonCommercial 4.0 license. The authors also acknowledge the NASA Prediction Of Worldwide Energy Resources project for providing open meteorological data.

Author contributions

J.C.: Conceptualization, Methodology, Software, Formal analysis, Validation, Visualization, Supervision, and Writing—review and editing. A.C.S.C.: Investigation, Data curation, Validation, Visualization, Writing—original draft, and Writing—review and editing. Both authors read and approved the final manuscript and accept responsibility for the work.

Funding

This research received no specific grant from any funding agency in the public, commercial, or not-for-profit sectors.

Competing interests

The authors have no relevant financial or non-financial interests to disclose.

Ethics approval

For the present secondary analysis, no additional ethics review was sought because the authors used openly available, aggregate, non-identifiable entomological occurrence records and had no contact with human participants or animals. The authors of this reanalysis did not conduct the original field collections. The source metadata describe protected human-attractant collections by trained personnel but do not provide an ethics-committee identifier or an individual-consent procedure; responsibility for the original collection protocol rests with the source study team.

Consent to participate and consent for publication

Not applicable to the present secondary analysis. No identifiable participant information is reported. The source metadata available to the reanalysis authors do not document the original consent procedure.

Data and code availability

The source entomological dataset is available from the Instituto Nacional de Salud through GBIF at https://doi.org/10.15472/kftrcn under CC BY-NC 4.0. Meteorological data were obtained from the NASA POWER Daily API at https://power.larc.nasa.gov/. The public version 1 reproducibility package is available in Mendeley Data (Ceballos and Silva 2026): https://doi.org/10.17632/x4ygk8vr64.1. A clean version 2 update containing the revised post-processing code, full-design collinearity results, spatial metric uncertainty, and consolidated outputs is prepared. The version-specific DOI in this statement and in the reference list must be changed only after version 2 is published.

References

1. Adde A, Roux E, Mangeas M, Dessay N, Nacher M, Dusfour I, Girod R, Briolant S (2016) Dynamical mapping of Anopheles darlingi densities in a residual malaria transmission area of French Guiana by using remote sensing and meteorological data. PLoS ONE 11:e0164685. https://doi.org/10.1371/journal.pone.0164685
2. Ahumada ML, Orjuela LI, Pareja PX, Conde M, Cabarcas DM, Cubillos EFG, Lopez JA, Beier JC, Herrera S, Quiñones ML (2016) Spatial distributions of Anopheles species in relation to malaria incidence at 70 localities in the highly endemic Northwest and South Pacific coast regions of Colombia. Malar J 15:407. https://doi.org/10.1186/s12936-016-1421-4
3. Ahumada ML, Vargas-García N, Ballesteros J, Díaz-Herrera T, Cotazo K, Vargas E, Alvarez-Fernández N, Moreno C, Calderón N, Aguirre J, Lucumí D, Vargas E, Levine R, Lenhart A, Morales CA, Herrera-Varela M (2021) Especies del género Anopheles (Diptera: Culicidae) asociadas al domicilio humano en 25 localidades de los municipios de Timbiquí, Guapi y Santa Bárbara ubicadas un área endémica para malaria al suroccidente de Colombia. Version 1.0. Instituto Nacional de Salud, occurrence dataset. https://doi.org/10.15472/kftrcn
4. Benjamini Y, Hochberg Y (1995) Controlling the false discovery rate: a practical and powerful approach to multiple testing. J R Stat Soc B 57:289–300. https://doi.org/10.1111/j.2517-6161.1995.tb02031.x
5. Cameron AC, Miller DL (2015) A practitioner's guide to cluster-robust inference. J Hum Resour 50:317–372. https://doi.org/10.3368/jhr.50.2.317
6. Ceballos J, Silva A (2026) Data and MATLAB code for species-specific hydroclimate associations and transferability of positive Anopheles catch intensity in southwestern Colombia. https://doi.org/10.17632/x4ygk8vr64.2. Mendeley Data, version 2

7. Escovar JE, González R, Quiñones ML (2013) Anthropophilic biting behaviour of Anopheles (Kerteszia) neivai Howard, Dyar & Knab associated with fishermen's activities in a malaria-endemic area in the Colombian Pacific. Mem Inst Oswaldo Cruz 108:1057–1064. https://doi.org/10.1590/0074-0276130256
8. Fuller DO, Ahumada ML, Quiñones ML, Herrera S, Beier JC (2012) Near-present and future distribution of Anopheles albimanus in Mesoamerica and the Caribbean Basin modeled with climate and topographic data. Int J Health Geogr 11:13. https://doi.org/10.1186/1476-072X-11-13
9. Meyer H, Reudenbach C, Hengl T, Katurji M, Nauss T (2018) Improving performance of spatio-temporal machine learning models using forward feature selection and target-oriented validation. Environ Model Softw 101:1–9. https://doi.org/10.1016/j.envsoft.2017.12.001
10. Montoya-Lerma J, Solarte YA, Giraldo-Calderón GI, Quiñones ML, Ruiz-López F, Wilkerson RC, González R (2011) Malaria vector species in Colombia: a review. Mem Inst Oswaldo Cruz 106(Suppl 1):223–238. https://doi.org/10.1590/S0074-02762011000900028
11. Mordecai EA, Caldwell JM, Grossman MK, Lippi CA, Johnson LR, Neira M, Rohr JR, Ryan SJ, Savage V, Shocket MS, Sippy R, Stewart Ibarra AM, Thomas MB, Villena O (2019) Thermal biology of mosquito-borne disease. Ecol Lett 22:1690–1708. https://doi.org/10.1111/ele.13335
12. Murillo C, Astaiza R, Fajardo P (1988) Biology of Anopheles (Kerteszia) neivai H., D. & K., 1913 (Diptera: Culicidae) on the Pacific coast of Colombia: I. Fluctuation of larval population and characteristics of the breeding places. Rev Saude Publica 22:94–100. https://doi.org/10.1590/S0034-89101988000200004
13. Naranjo-Díaz N, Altamiranda M, Luckhart S, Conn JE, Correa MM (2014) Malaria vectors in ecologically heterogeneous localities of the Colombian Pacific region. PLoS ONE 9:e103769. https://doi.org/10.1371/journal.pone.0103769
14. NASA POWER Project (2026) NASA Prediction Of Worldwide Energy Resources (POWER) Daily API. NASA Langley Research Center. https://power.larc.nasa.gov/. Accessed 31 August 2026
15. Piedrahita S, Altamiranda-Saavedra M, Correa MM (2020) Spatial fine-resolution model of malaria risk for the Colombian Pacific region. Trop Med Int Health 25:1024–1031. https://doi.org/10.1111/tmi.13443
16. Roberts DR, Bahn V, Ciuti S, Boyce MS, Elith J, Guillera-Arroita G, Hauenstein S, Lahoz-Monfort JJ, Schröder B, Thuiller W, Warton DI, Wintle BA, Hartig F, Dormann CF (2017) Cross-validation strategies for data with temporal, spatial, hierarchical, or phylogenetic structure. Ecography 40:913–929. https://doi.org/10.1111/ecog.02881
17. Ruiz D, Poveda G, Vélez ID, Quiñones ML, Rúa GL, Velásquez LE, Zuluaga JS (2006) Modelling entomological-climatic interactions of Plasmodium falciparum malaria transmission in two Colombian endemic regions: contributions to a national malaria early warning system. Malar J 5:66. https://doi.org/10.1186/1475-2875-5-66
18. Solarte Y, Hurtado C, González R, Alexander B (1996) Man-biting activity of Anopheles (Nyssorhynchus) albimanus and An. (Kerteszia) neivai (Diptera: Culicidae) in the Pacific lowlands of Colombia. Mem Inst Oswaldo Cruz 91:141–146. https://doi.org/10.1590/S0074-02761996000200002
19. Wenger SJ, Olden JD (2012) Assessing transferability of ecological models: an underappreciated aspect of statistical validation. Methods Ecol Evol 3:260–267. https://doi.org/10.1111/j.2041-210X.2011.00170.x
20. Wieczorek J, Bloom D, Guralnick R, Blum S, Döring M, Giovanni R, Robertson T, Vieglais D (2012) Darwin Core: an evolving community-developed biodiversity data standard. PLoS ONE 7:e29715. https://doi.org/10.1371/journal.pone.0029715
21. Zeileis A, Kleiber C, Jackman S (2008) Regression models for count data in R. J Stat Softw 27:1–25. https://doi.org/10.18637/jss.v027.i08

Figures

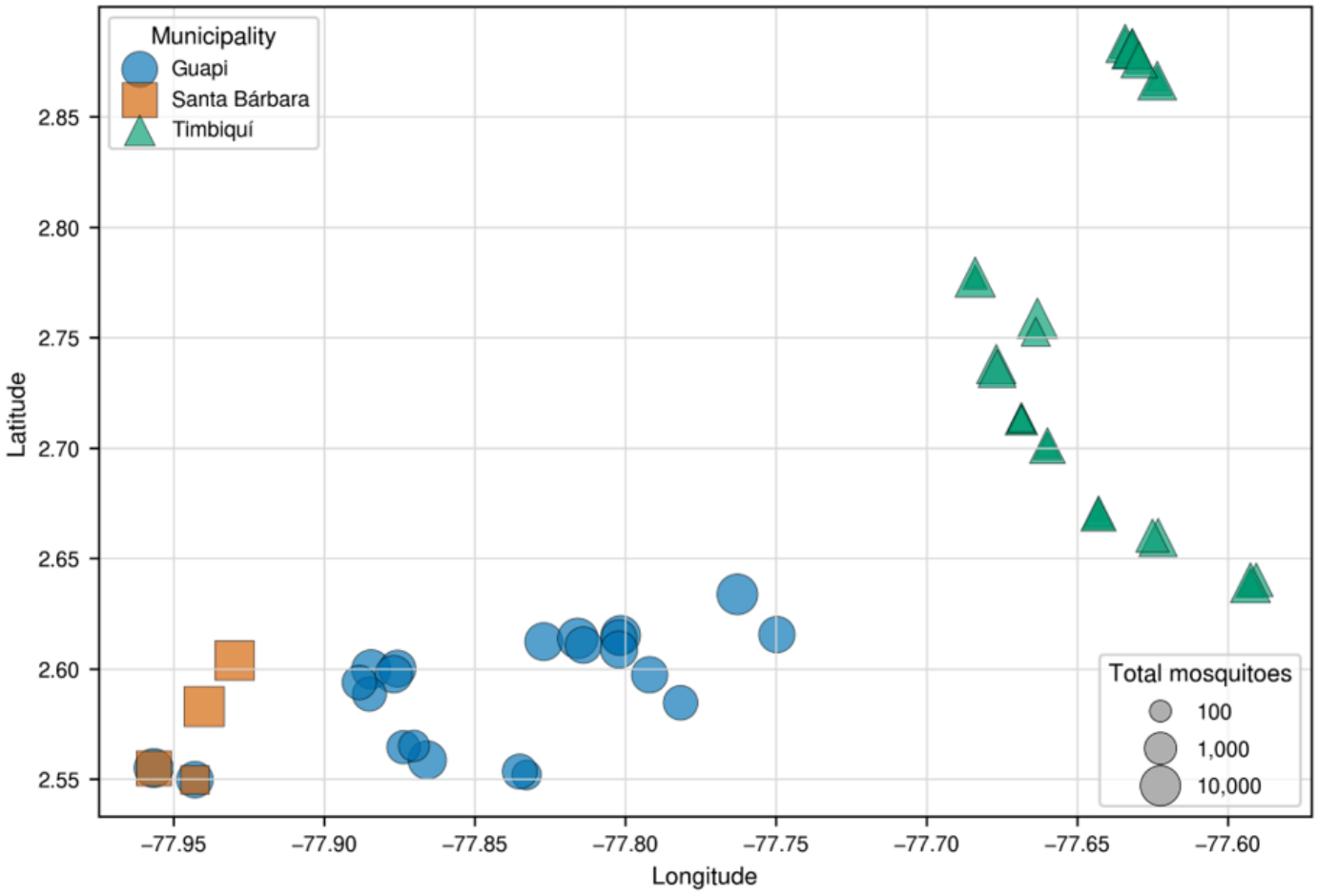


Figure 1

Spatial support of published sampling units. Each point represents a parentEventID–coordinate pair; point area is proportional to log(1 + total individualCount), with reference sizes shown in the legend, and marker symbol denotes municipality. No basemap was added, so the figure depends only on published coordinates

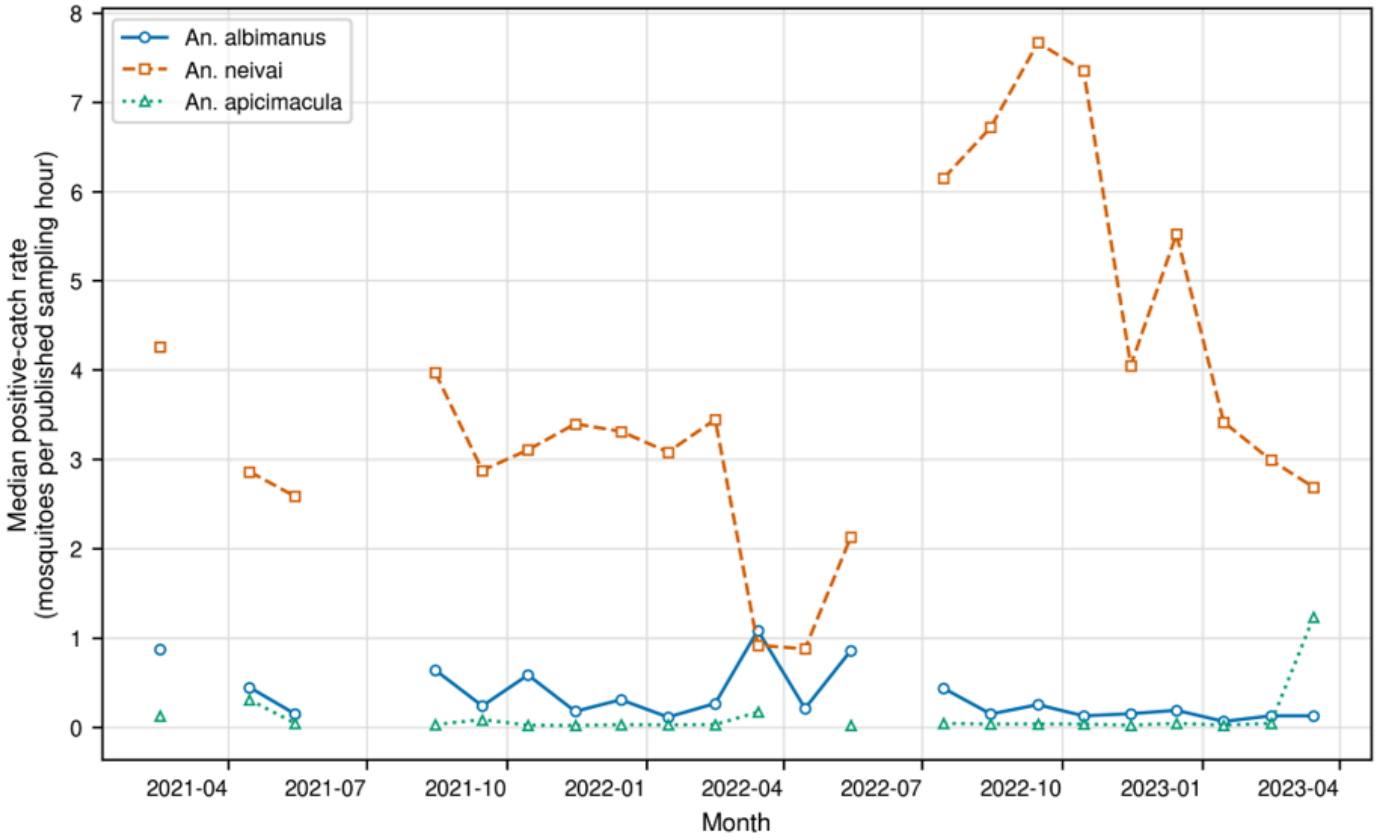


Figure 2

Monthly median positive-catch rate by species. Points summarize months represented in the source records; connecting segments are descriptive and do not imply observations during unsampled intervals. *Anopheles apicimacula* is shown descriptively but was excluded from modelling by the prespecified gate

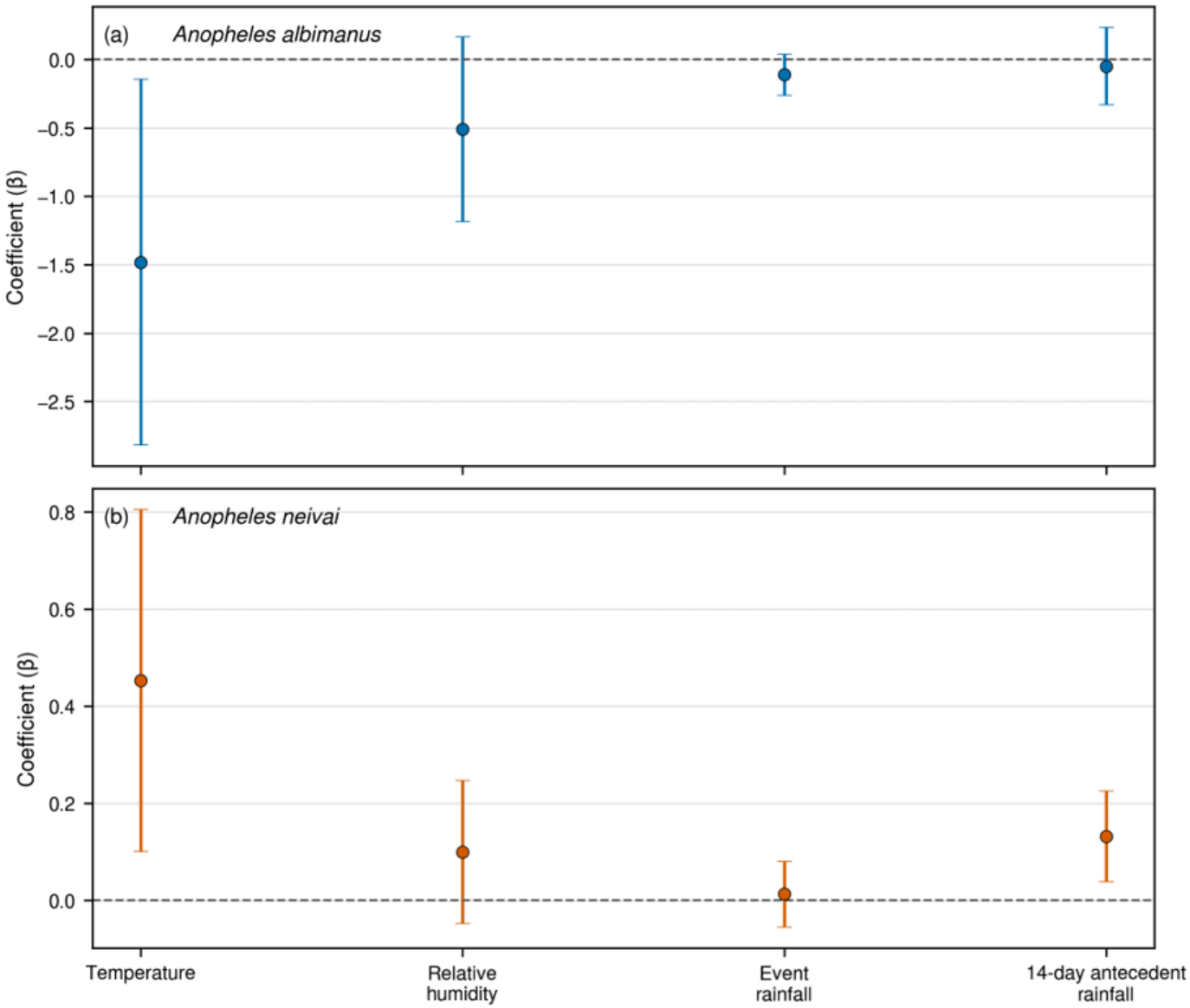


Figure 3

Standardized hydroclimate coefficients and unadjusted cluster-robust 95% confidence intervals from the final all-year zero-truncated negative binomial models. The dashed horizontal line marks beta = 0; corresponding raw p values and Benjamini–Hochberg q values are reported in Table 2

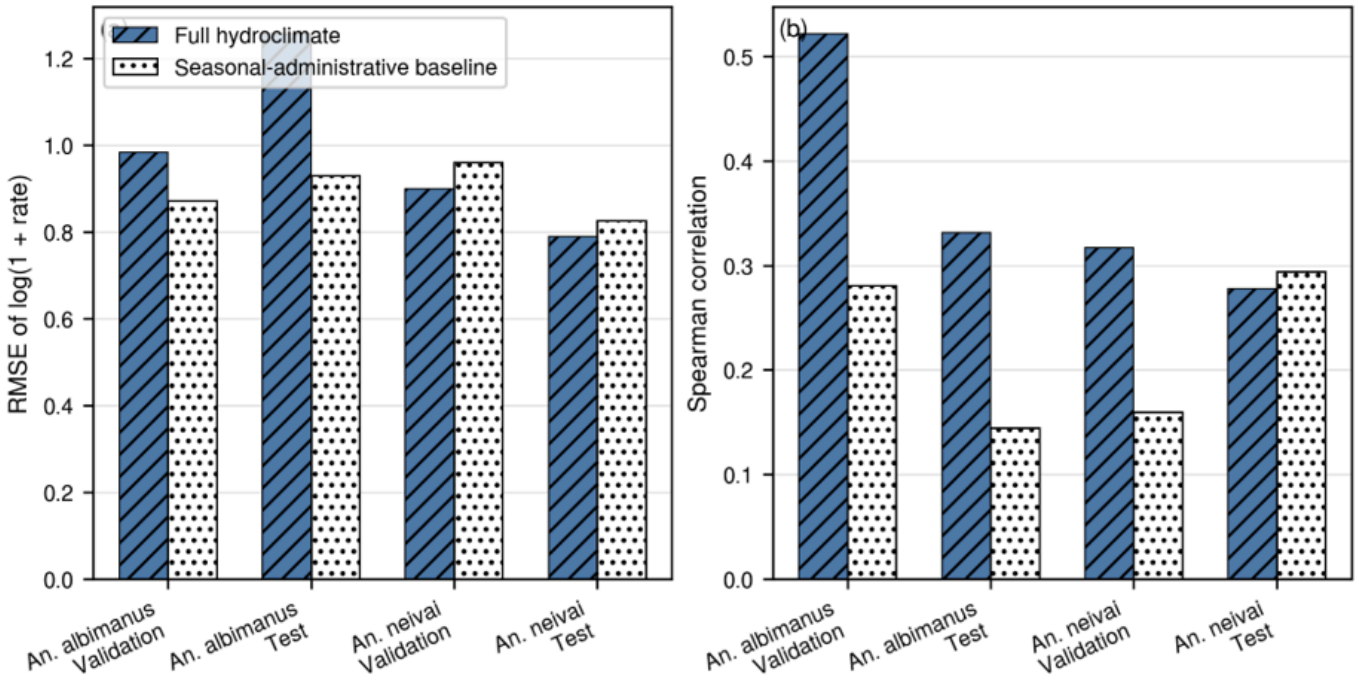


Figure 4

Frozen temporal validation in 2022 and January–March 2023. Paired bars compare the full hydroclimate model with the seasonal–administrative baseline. The left panel shows root mean squared error of log(1 + positive-catch rate); the right panel shows Spearman rank correlation. Bars are descriptive point estimates from the single frozen split; no uncertainty interval was prespecified. Hatching preserves model identification in grayscale reproduction

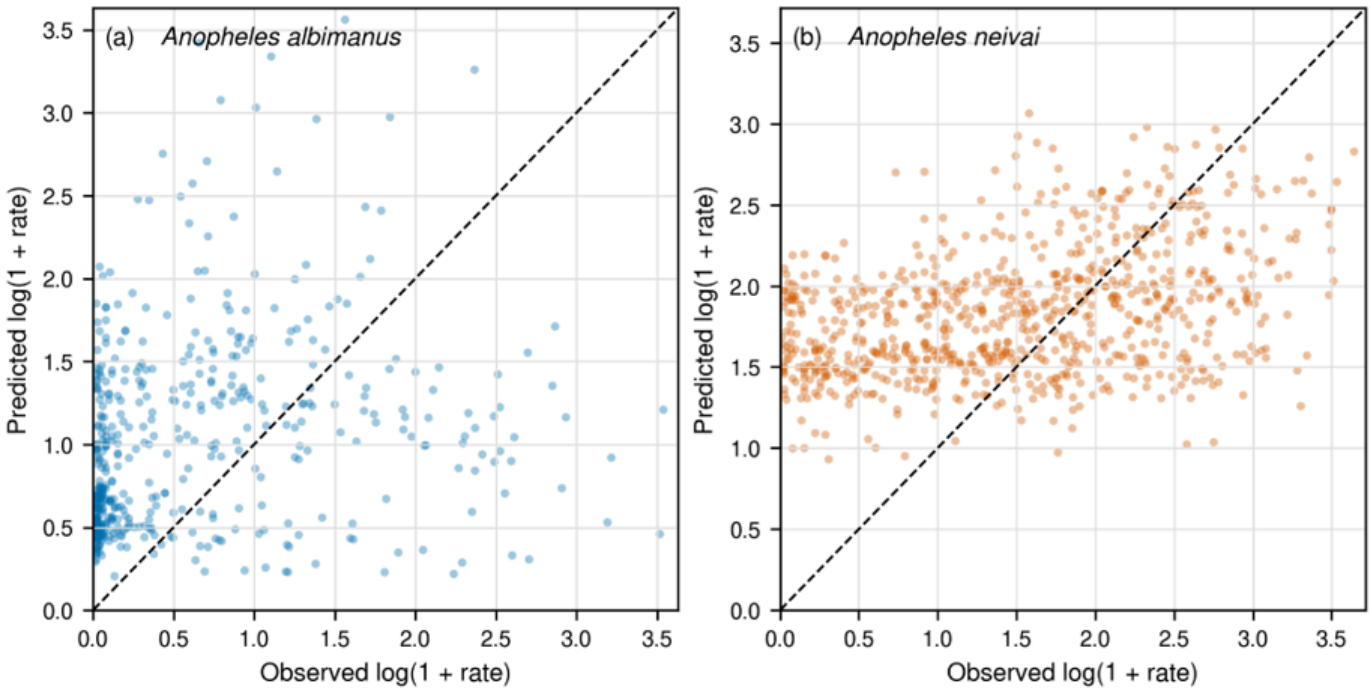


Figure 5

Observed versus predicted log(1 + positive-catch rate) under leave-one-parentEventID-out transfer. The dashed line is the 1:1 line. Dispersion around the line and compression of predicted values show limited unit-to-unit transfer, especially at extreme observed rates

Supplementary Files

This is a list of supplementary files associated with this preprint. Click to download.

- ESM1SupplementaryTablesFINAL.pdf
- ESM2MachineReadableResultsFINAL.zip
- ESM3SupplementaryFigureS1FINAL.pdf